Aalborg Universitet

AALBORG UNIVERSITY

Frequency Stability of Hierarchically Controlled Hybrid Photovoltaic-Battery-Hydropower Microgrids

Guan, Yajuan; Vasquez, Juan Carlos; Guerrero, Josep M.; Wu, Dan; Feng, Wei; Wang, Yibo

Frequency Stability of Hierarchically Controlled Hybrid Photovoltaic-Battery-Hydropower Microgrids

Yajuan Guan, Juan C. Vasquez, Josep M. Guerrero, Dan Wu

Research Programme on Microgrids www.microgrids.et.aau.dk
Department of Energy Technology Department
Aalborg University, Denmark
ygu@et.aau.dk

Wei Feng, Yibo Wang
Institute of Electrical Engineering
Chinese Academy of Sciences
Beijing, China

Abstract—**Hybrid photovolvaic battery-hydropower microgrids can increase electricity accessibility and availability in remote areas. In those microgrids with grid-connected and islanded modes capabilities, seamless transition between both modes is needed as well. However, the different resources with conventional constant P/Q and P/V controls coexisting in the microgrid may affect frequency stability. In this paper, a hierarchical control is proposed to perform power sharing among PV voltage source inverters (VSIs), while injecting the dispatched power to the main grid. Further, frequency stability analysis is presented based on small signal models of the hybrid PV-HP microgrid, including 2 MWp PV station, 15.2 MWh battery storage system, and 12.8 MVA hydropower plant. Simulation results of the microgrid and experimental results on a scaled-down laboratory prototype verify the effectiveness of the proposed hierarchical controller.**

Keywords: **Hybrid hydro-PV microgrid, hierarchical control, frequency stability**

I. INTRODUCTION

NOWADAYS, the electrical grid is progressing towards a more decentralized architectures and operation, thus reducing the dependency on centralized power plants. One promising decentralized power architecture is the Microgrid (MG), which usually involves different kinds of energy sources, such as wind or photovoltaic (PV) energy. Microgrids are local distribution grids including different technologies such as power electronics, distributed generation (DG), energy storage systems (ESSs), control, and communications [1], [2]. Hybrid PV-ESS-hydropower microgrids have been deployed as a reasonable solution to address local electricity shortages, eliminate power fluctuation, while increasing reliability and availability of power supply, especially in dry seasons. Further, hybrid PV-hydropower microgrids can increase the complementary use of different renewable energy sources in some remote area with abundant in solar irradiance, but with small scale hydroelectric power plants available [3], [4].

Microgrids in remote areas, due to the weakness of the grid, require seamless transition between grid-connected and islanded modes. At the same time, PV inverters should provide constant active and reactive powers (P/Q nodes), while hydropower present constant P and voltage (P/V node), which is hard to achieve by the conventional inverters connected to the hybrid microgrid system.

To cope with this problem, hierarchical control theory applied to microgrids can be used, thus providing functionalities defined in the different control levels [5], [6]. This way, hierarchical control can realize power sharing performance among PV voltage source inverters (VSIs), while injecting dispatched power to grid. Deploying hierarchical control strategies on PV plant may improve the capacity of the microgrid regarding power flow control, while increasing reliability of supply electrical power to local critical loads on device level [7].

Furthermore, inertia of hydraulic turbines and generators, decided by their dimension and weight, is an inherent property of a rotating device which could increase damping performance [8]. However, power-electronics-based microgrid may be sensitive to oscillations resulting from network disturbances due to absence of physical inertias. In addition, the multiple parameters of the hierarchical control need to be designed respecting trade-offs and bandwidth.

In view of these problems, stability analysis becomes an important issue in hybrid PV-hydro microgrids. In [9], the transient stability analysis of a hybrid microgrid is obtained from the relationship among the rotor angle of the different sources. In addition, operational characteristics of hybrid microgrids and stability analysis are presented as well in [10]-[11]. However there is no quantitative conclusion derived in these research works.

In many previous works, stability analysis based on eigenvalues and root locus plots is often presented. For instance, in [12] a full order small signal model of a droop controlled microgrid is derived to analyze the system stability.
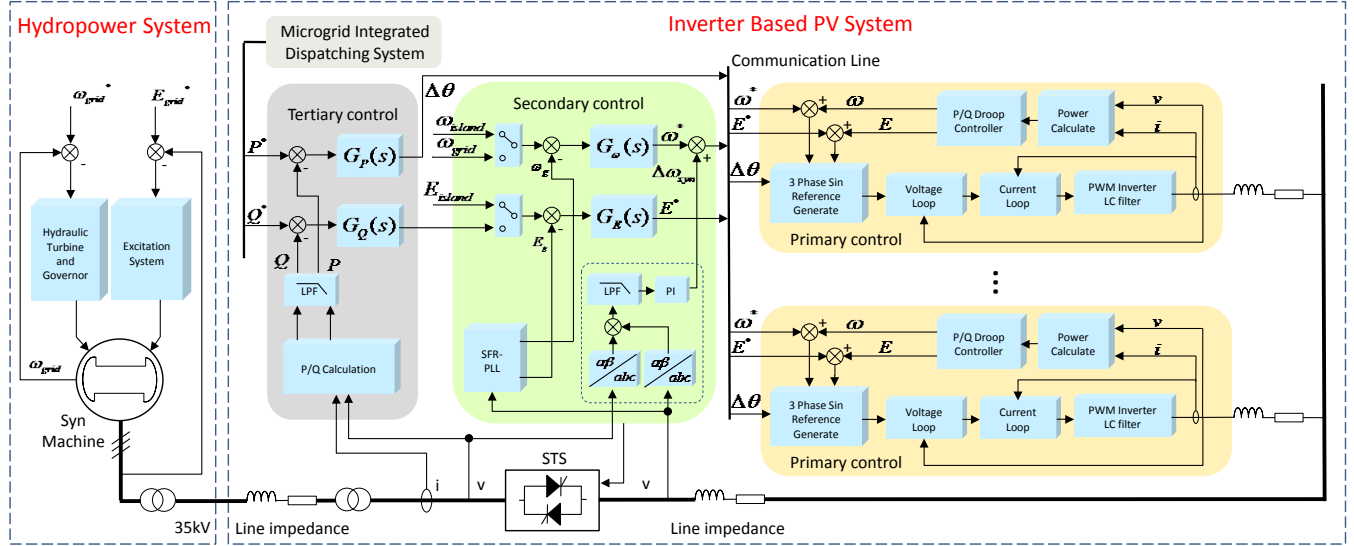
Fig.1. Block diagram of the hybrid microgrid control.

However in these works, inverters only operate in islanded mode and the characteristics of the generator is not considered. In contrast, in [13] the small-signal model of a synchronous generator was considered. Nevertheless, the dynamic response of a hydroelectric power station should be taken into account, since the characteristic of the prime mover and its governor have great influence on the features of the local electrical network [14].

In this paper, a hierarchical controller is proposed to realize the power sharing performance among PV-based VSIs, while dispatching power to the grid. Root locus analysis is presented based on state space models of the hybrid PV-battery-hydropower microgrid to analize the system stability. Simulation results are done in order to verify system frequency stability by using a demonstration platform of a hybrid microgrid consisted of a 2 MWp PV station, a 15.2 MWh battery storage system, and a 12.8 MVA hydropower station. Experimental results on a scale-down laboratory prototype verify the effectiveness of the hierarchical control.

II. CONFIGURATION OF THE HYBRID POWER SYSTEM

The model of the hybrid PV-battery-hydropower microgrid system under study oriented to the frequency stability is shown in Fig 1. The synchronous generator of the hydropower plant provides real inertia, which is differs from conventional power-electronics-based microgrid systems.

In our case, the synchronous generator works in standalone mode, which means that the main function of the hydraulic governor and excitation system is to maintain the frequency and amplitude of the microgrid when it is operating in islanded mode, i.e. disconnected from the main grid. Therefore, the hydropower system acts like a P/V node from the viewpoint of the microgrid. Since the system frequency stability is the main concern of this paper, the output voltage amplitude of hydropower plant is set to a constant and the influence of voltage fluctuations are neglected based on the assumption that excitation control loop is properly designed.

The PV plant can be self-controlled based on a hierarchical control that can be divided into three levels [5].

i) *Primary control level* consists of inner voltage and current control loop, virtual impedance control loop, and P and Q droop control loop. Their objectives are tracking voltage command, adjusting R/X ratio of the impedance 'seen' by the inverter, and sharing the load among VSIs by mimicking the static droop feature of a synchronous generator.

ii) *Secondary control level* includes frequency and amplitude restoration control loop and synchronization control loop. It can compensate frequency and amplitude deviations from the normal value to improve the power supply quality in standalone mode and to synchronize VSIs' voltage to grid voltage at the static transfer switch (STS).

iii) *Tertiary control level* is responsible to set the power command and control VSIs to inject dispatched power to the grid, as well as to optimize the system.

Therefore, the whole PV plant of the hybrid power system can be seen as a P/Q node. The output voltages of PV system and hydropower system are boosted to 35 kV through transformers and the transmission lines between plants present high X/R ratio. Therefore, we can consider a very inductive line X, so that P and Q are dominated by the power angle (δ) and the voltage difference ($U_1 – U_2$), respectively:

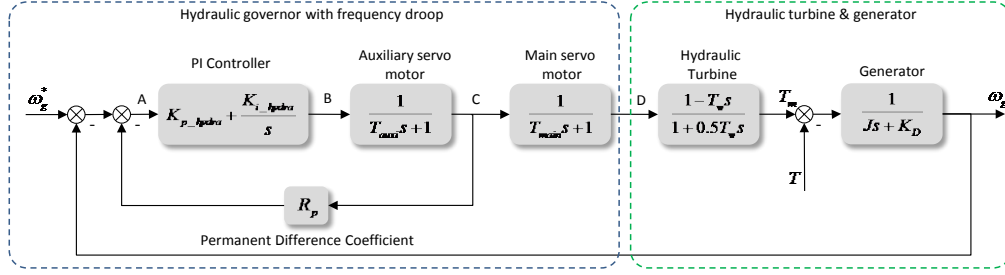$$\delta \approx \frac{XP}{U_1U_2} \qquad (1)$$

Fig.2. Block diagram of the hydraulic governor control.

$$U_1 - U_2 \approx \frac{XQ}{U_1} \qquad (2)$$

where the δ is the angle between hydropower and PV systems, X is the line impedance, P and Q are the output active and reactive power, U_1 and U_2 are the output voltages of hydropower and PV systems.

On the other hand, the frequency of the hydropower plant is mainly dominated by the hydraulic governor system and active power demanded by the grid. Therefore, the frequency stability analysis in this paper is focused on study the relationship between the power flow controller of paralleled PV-based VSIs and the governor system of the hydropower station.

III. LINEARIZED SYSTEM MODEL

A. Model of the hydraulic governor

The function of auxiliary and main servo motors is to amplify impeller driving signal from a PI controller. The impeller controls the water inflow in order to stabilize generator's frequency indirectly. The governor allows parallel operation by using $P–\omega$ droop via permanent difference coefficient R_p. The control scheme of the hydraulic governor is depicted in Fig. 2.

The differential equation of the PI and the $P–\omega$ droop controls can be expressed as:

$$pB = -K_{p\_hydra} p\omega_g - K_{p\_hydra} R_p pC + K_{i\_hydra} \omega_g^* \\ -K_{i\_hydra}\omega_g - K_{i\_hydra}R_p C \qquad (3)$$

where the Laplace operator p represents a derivative term. The auxiliary and main servo motors can be described separately as follows

$$pC = \frac{1}{T_{auxi}} B - \frac{1}{T_{auxi}} C \qquad (4)$$

$$pD = \frac{1}{T_{main}} C - \frac{1}{T_{main}} D . \qquad (5)$$

Hydraulic turbine is simplified by a non-minimum phase system with a positive zero-pole at $(1/T_w, 0)$, which describes the water hammer phenomenon happened in a non-elastic water column, as follows:

$$pT_m = (\frac{2}{T_w} + \frac{2}{T_{main}})D - \frac{2}{T_{main}}C - \frac{2}{T_w}T_m . \qquad (6)$$

The generator is modelled based on a kinetic equation with rotary inertia J and self-balancing coefficient K_D, as following:

$$p\omega_g = \frac{1}{J}(T_m - T - K_D\omega_g) \qquad (7)$$

B. Model of the PV system

The $P-\omega$ droop controller of VSI where performed as follows:

$$\omega = \omega_{grid} + \Delta\omega_{syn} - m_p(P^* - P) \qquad (8)$$

$$\theta = \int \omega dt + \Delta\theta \qquad (9)$$

where m_p is the $P-\omega$ droop coefficient; $\Delta\omega_{syn}$ is a signal generated by the synchronization controller in the secondary level in order to ensure the synchronization before connecting the VSIs to hydropower grid; ω_{grid} is the fundamental value of $P-\omega$ droop controller; P^* is the power reference; $\Delta\theta$ is generated by a PI controller in the tertiary control to ensure VSIs can dispatch power into grid.

The behavior of the primary level could be recognized as a voltage servo system, with specific time delay ω_{inv} determined by the voltage/current control parameters, as well as the LC filter. The power transmitted from the PV system to the hydropower system depends on the power transmission model.

The delay time of inverter voltage and current control loop can be ignored when comparing to governor dynamics of the hydropower system. Therefore, VSI can be simplified as shown in Fig. 3. In this figure, K_{p_inv} and K_{i_inv} are the parameters of PI controller of the tertiary control. The inner loop of VSI can be equivalent to a low pass filter with a bandwidth T_{inv}.
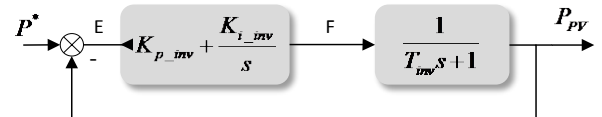

Fig.3. Simplified control block diagram of PV system.

The model of the PV system can derived as follows:

$$pF = -K_{p\_inv}pP_{PV} + K_{i\_inv}P^* - K_{i\_inv}P_{PV} \qquad (10)$$

C. Model of transformation and integration

A mathematical transformation is necessary to combine the hydropower and PV system models. The transformation, which is based on represent the active power as the torque in the rotor kinetic equation, can be written as:

$$T_{INV} = \frac{P_{PV}}{2\pi\omega_g}\frac{\omega_{base}}{VA_{base}} \qquad (11)$$

where ω_{base} and ω_g is the basic and real value of system angle frequency, respectively; and VA_{base} is the total capacity of hybrid system.

The model of the PV system can be integrated together with the hydropower model by means of

$$T = T_{INV} - T_e \qquad (12)$$

where T_e represents the total active power load in the grid, transformed to torque by means of (11). The transformation model is shown in Fig.4.

Based on (3) to (12), the state space model can be derived as

$$\overrightarrow{x_{sys}} = Ax_{sys} + Bu \qquad (13)$$

where $x_{sys} = \begin{bmatrix} \Delta B & \Delta C & \Delta D & \Delta P_{PV} & \Delta F & \Delta\omega_g & \Delta T_m \end{bmatrix}^T$, and the state matrix, input matrix and input variables are shown in the top of next page.

IV. SYSTEM STABILITY ANALYSIS BASED ON LINEARIZED MODEL TEMPLATE

The frequency stability of hydro-PV hybrid microgrid in this Section is analysed through root locus based on system state space models, with the parameters given in Table I.

Fig. 5(a) shows that as K_{p_inv} increases, modes λ_6 and λ_7 move towards real axis. It can be observed that the imaginary part of eigenvalues became zero, thus the two eigenvalues separate along the real axis. Fig. 5(b) shows that as K_{i_inv} increases, firstly modes λ_6 and λ_7 get close along real axis, and then apart in vertical direction, which means that the system is becoming more oscillatory.
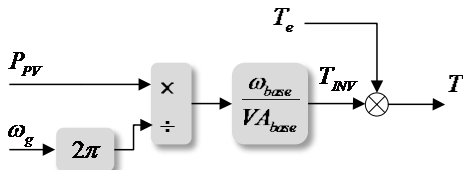

Fig.4. Control block diagram of transform model.

Parameters	Values	Parameters	Values
ω_g	1.0	J	10.0
K_{i_hydra}	0.7	K_d	4.0
K_{p_hydra}	3.0	K_{i_inv}	10.0
R_p	0.005	K_{p_inv}	2.0
T_{auxi}	0.05	ω_{base}	314 rad/s
T_{main}	0.1	VA_{base}	17.8 MVA
T_w	2.0	T_{inv}	0.2 s

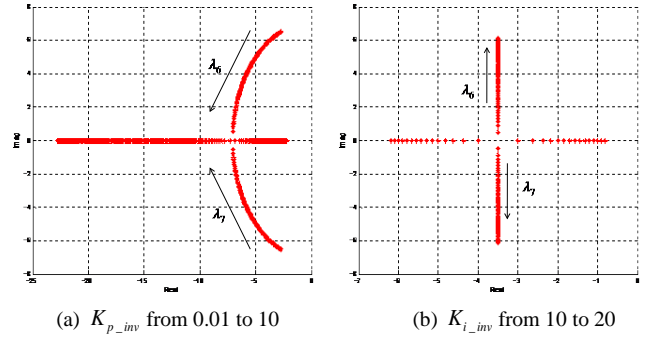(a) K_{p_inv} from 0.01 to 10   (b) K_{i_inv} from 10 to 20

Fig.5. Trace of modes as a function of K_{p_inv} and K_{i_inv}

By increasing delay time of the inverter equivalent system, which consist of the dynamic response time of secondary and primary control loop, as well as the bandwidth of communication for hierarchical control, will make system more unstable. Latent roots λ_6 and λ_7 become poor damped, and λ_5 gets closer to imaginary axis, as shown in Fig.6.

The control parameters of the hydraulic governor will also significantly influence the frequency stability. Fig. 7 (a) shows that as K_{i_hydra} increases, modes λ_3 and λ_4 are getting closer to the imaginary axis. When K_{p_hydrau} increases, modes λ_5, λ_3, and λ_4 are also getting closer to the imaginary axis, which will deteriorate the damping performance.
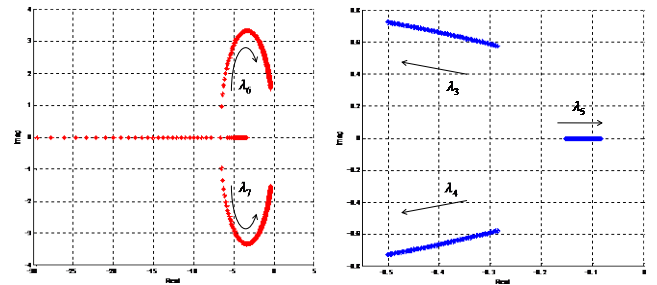

Fig. 6. Trace of modes in function of T_{inv} : T_{inv} from 0.01 to 2.

$$A = \begin{bmatrix} -\dfrac{K_{p\_hydra}R_p}{T_{auxi}} & \dfrac{K_{p\_hydra}R_p}{T_{auxi}} - K_{i\_hydra}R_p & 0 & -\dfrac{K_{p\_hydra}\omega_{base}}{2\pi JVA_{base}\omega_g} & 0 & \dfrac{K_{p\_hydra}T_{inv}}{J\omega_g} + \dfrac{K_{p\_hydra}K_D}{J} - K_{i\_hydra} & -\dfrac{K_{p\_hydra}}{J} \\[3mm] \dfrac{1}{T_{auxi}} & -\dfrac{1}{T_{auxi}} & 0 & 0 & 0 & 0 & 0 \\[3mm] 0 & \dfrac{1}{T_{main}} & -\dfrac{1}{T_{main}} & 0 & 0 & 0 & 0 \\[3mm] 0 & 0 & 0 & -\dfrac{1}{T_{inv}} & \dfrac{1}{T_{inv}} & 0 & 0 \\[3mm] 0 & 0 & 0 & \dfrac{K_{p\_inv}}{T_{inv}} - K_{i\_inv} & -\dfrac{K_{p\_inv}}{T_{inv}} & 0 & 0 \\[3mm] 0 & 0 & 0 & \dfrac{\omega_{base}}{2\pi JVA_{base}\omega_g} & 0 & -\dfrac{T_{inv}}{J\omega_g} - \dfrac{K_D}{J} & \dfrac{1}{J} \\[3mm] 0 & -\dfrac{2}{T_{main}} & \dfrac{2}{T_w} + \dfrac{2}{T_{main}} & 0 & 0 & 0 & -\dfrac{2}{T_w} \end{bmatrix}$$

$$B = \begin{bmatrix} \dfrac{K_{p\_hydra}}{J} & K_{i\_hydra} \\[3mm] 0 & 0 \\[1mm] 0 & 0 \\[1mm] 0 & 0 \\[1mm] 0 & 0 \\[1mm] -\dfrac{1}{J} & 0 \\[3mm] 0 & 0 \end{bmatrix} \qquad u = \begin{bmatrix} \Delta T_e \\[2mm] \Delta \omega_g^* \end{bmatrix}$$

Fig.8. Electrical diagram of the hybrid microgrid.

In Fig. 8 parameters of tertiary controller of the PV inverter system are calculated and selected based on the abovementioned stability analysis results. In order to test the stability of the whole system, disturbances such as PV station and load connection/disconnection, or solar irradiance suddenly dropped were include, resulting in the following results.

Fig. 9(a) shows the transient response of system frequency when a 2 MW load is connected the hybrid system at t=500s. After 150s of oscillation, the system frequency finally is stabilized at 49.55 Hz. Fig. 9(b) shows the transient response of system frequency when a 2 MW load is disconnected from the hybrid system at t=500s. After 200s of oscillation, the system frequency finally restored back to 50Hz.

Fig. 10(a) shows the transient response of system frequency when solar irradiance suddenly dropped to 30% at t=510s. After about 150s oscillation, the system frequency finally stabilized at 49.905Hz, which means that the frequency deviation after disturbance is just 0.02% (0.01Hz). Fig. 10(b) shows the transient response of output power of one parallel PV station, when solar irradiance suddenly dropped to 30% at t=510s. Notice that the output active power of the PV station is reduced by 6.79% (67.9 kW) and the output reactive power is reduced by 2.66% (77.6 kVar) at 510s. After about 3s oscillation, the output active power is restored to the nominal value due to the discharge of the battery storage system.
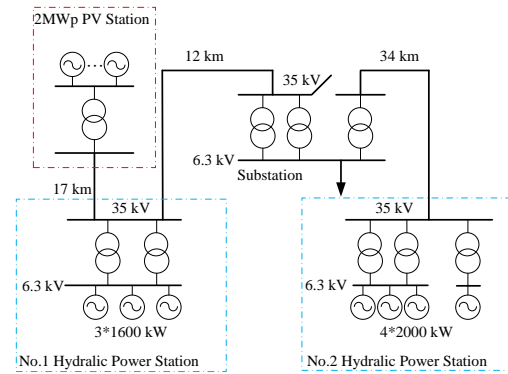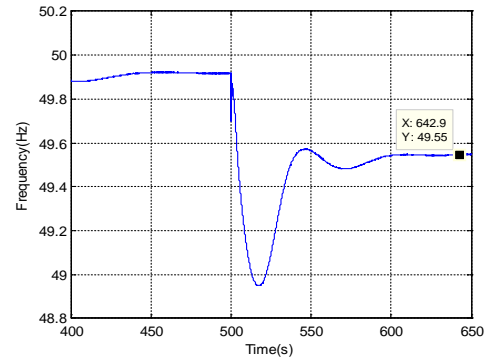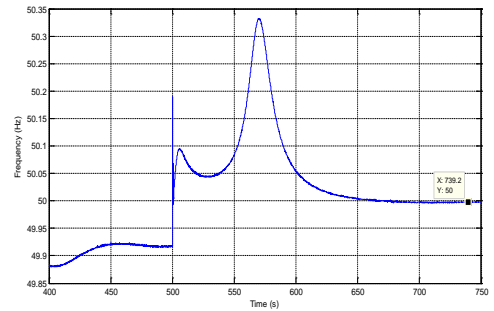

(a) Load connection

(b) Load disconnection

Fig.9. Transient response of system frequency.

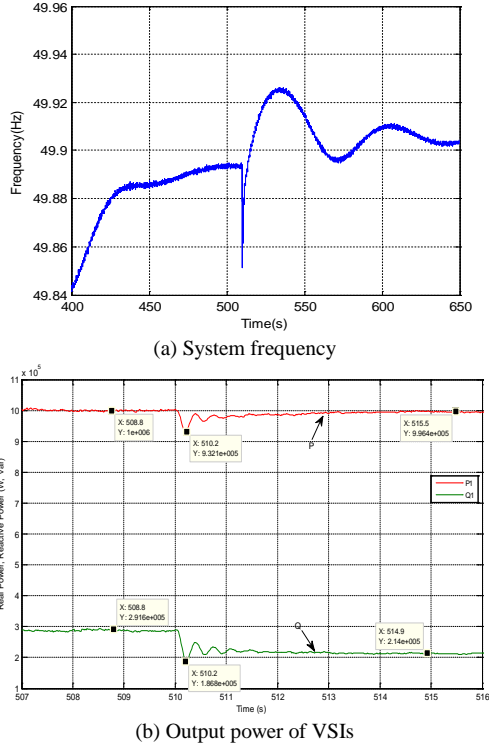(a) System frequency

(b) Output power of VSIs

Fig.10. Transient response during suddenly dropped solar irradiance

V. SIMULATION AND EXPERIMENTAL RESULTS OF HIERARCHICAL CONTROL THE HYBRID MICROGRID

In order to verify the effectiveness of the hierarchical controller and its effects on hybrid power system frequency, a scale-down laboratory prototype is built according to Fig.1. The experimental setup consists of two Danfoss 2.2 kW inverters, a dSPASE1006 control board, LCL filters, LEM sensors and two resistive loads, as shown in Fig.11. One of the inverter is used to simulate the hydropower. The other employs the droop controller and hierarchical controller to simulate the VSI interfaced PV/battery hybrid system. The electrical setup and control system parameters are listed in Table I and II.

The time-domain model of the proposed control scheme is developed to evaluate the performances in Matlab/Simulink environment.

TABLE III
SYSTEM PARAMETERS OF PROPOSED CONTROLLER

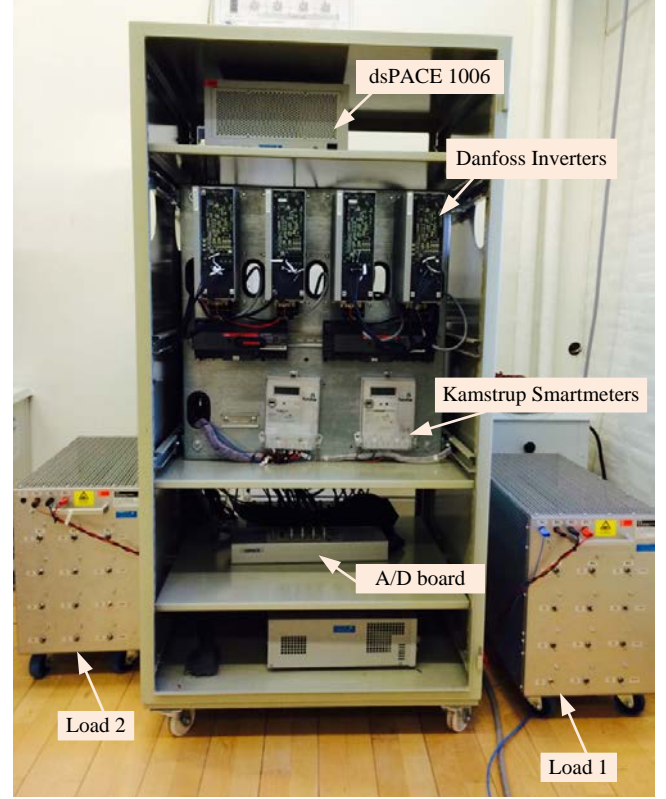| Parameter	Value	Parameter	Value	Parameter	Value
k_{pv}	0.01	k_{pq}	5e-5	k_{ii}	0.052
k_{iv}	50	k_{iq}	5e-4	k_{pp}	10e-6
k_{ip}	5e-5	P^*	275 W	Q^*	0 kVar

Fig. 11. Experimental setup.

Fig.12 shows the experimental results of the transient response of the system frequency and output active power of hydropower and PV system when the PV system is connecting to the hydropower plant. After 40 seconds, the output active power of PV system reached the reference value given by the hierarchical controller. The hydropower frequency increased due to the compensation of the PV system.

Fig.13 shows the experimental results of the transient response of the system frequency and output power of hydropower and PV system when the PV system is disconnecting from the hydropower plant. The output active power of PV system is decreased in order to supply only the local load. At the same time, the output active power of hydropower is increased to 300W, which also increases the hydropower frequency drop.

Figs.14 and 15 show the experimental results of the transient response of the output active power of hydropower plant and the PV system during the hydropower-side load connection/disconnection. It can be seen that the hydropower output power increases immediately. However, the PV system output-power is almost constant, being barely affected by the hydropower-side load disturbance.
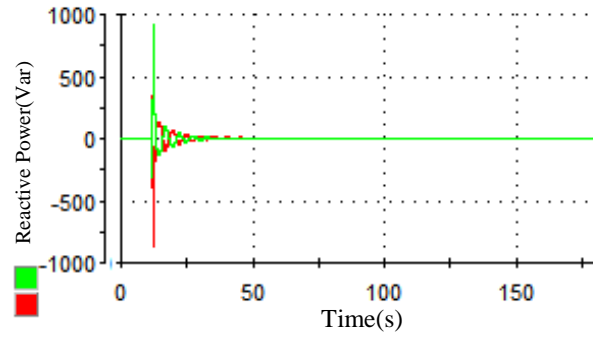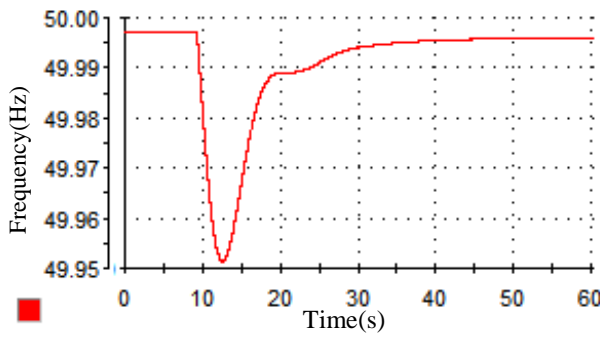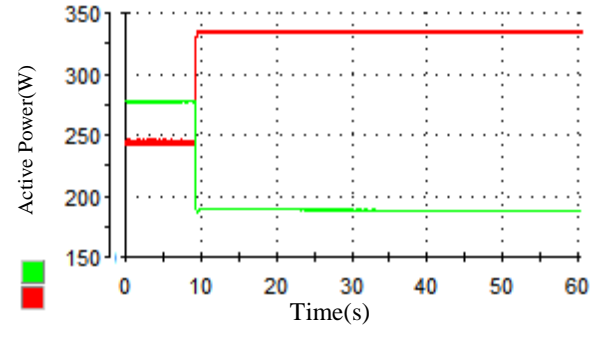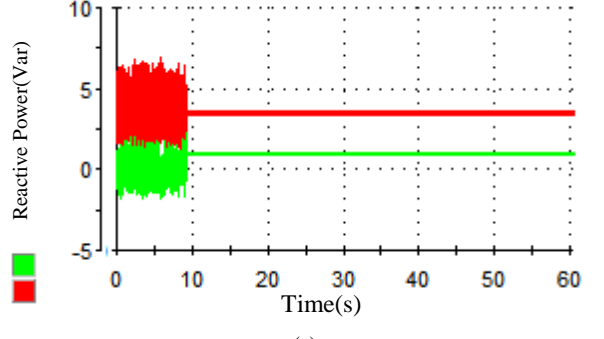
(a)

(b)

(b)

(c)
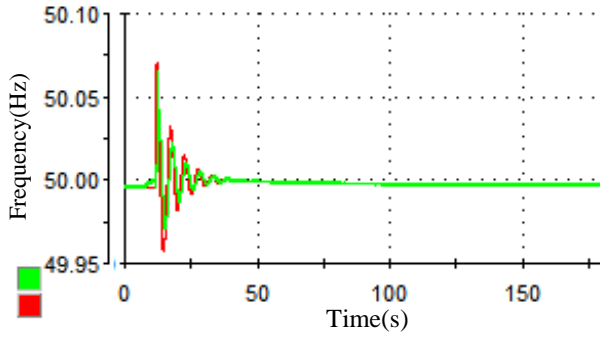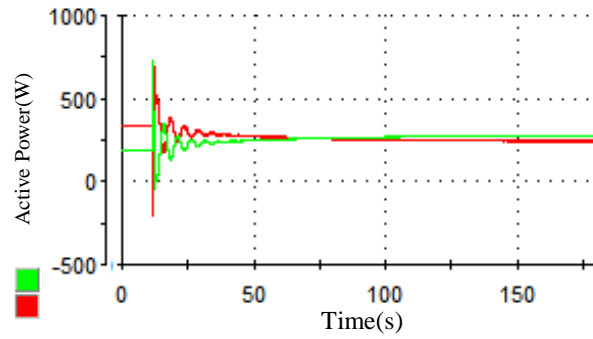
(c)

Fig.12. Experimental results of transient response when PV system is connected to the hydropower: (a) frequency; (b) active power sharing; (c) reactive power sharing. Hydropower (red) and PV system (green)
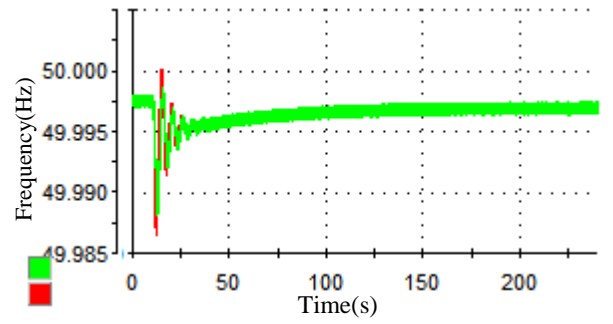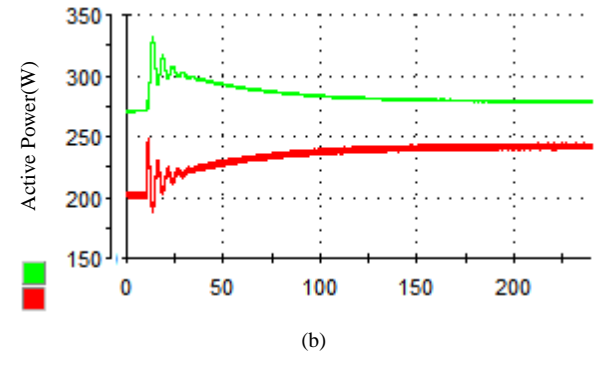
Fig. 13. Experimental results of transient response when PV system is disconnecting from the hydropower: (a) frequency; (b) active power sharing; (c) reactive power sharing. Hydropower (red) and PV system (green).
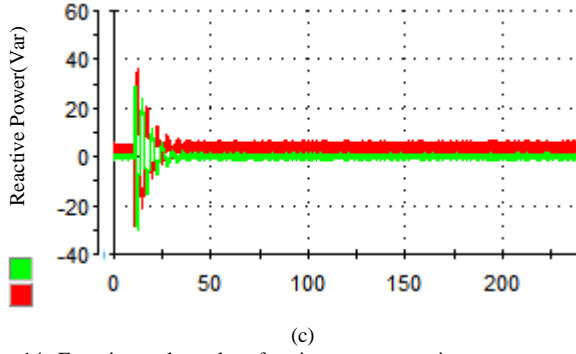

(a)

(a)

(b)

(c)

Fig. 14. Experimental results of active power transient responses during load connection disturbance: (a) frequency; (b) active power sharing; (c) reactive power sharing. Hydropower (red) and PV system (green)
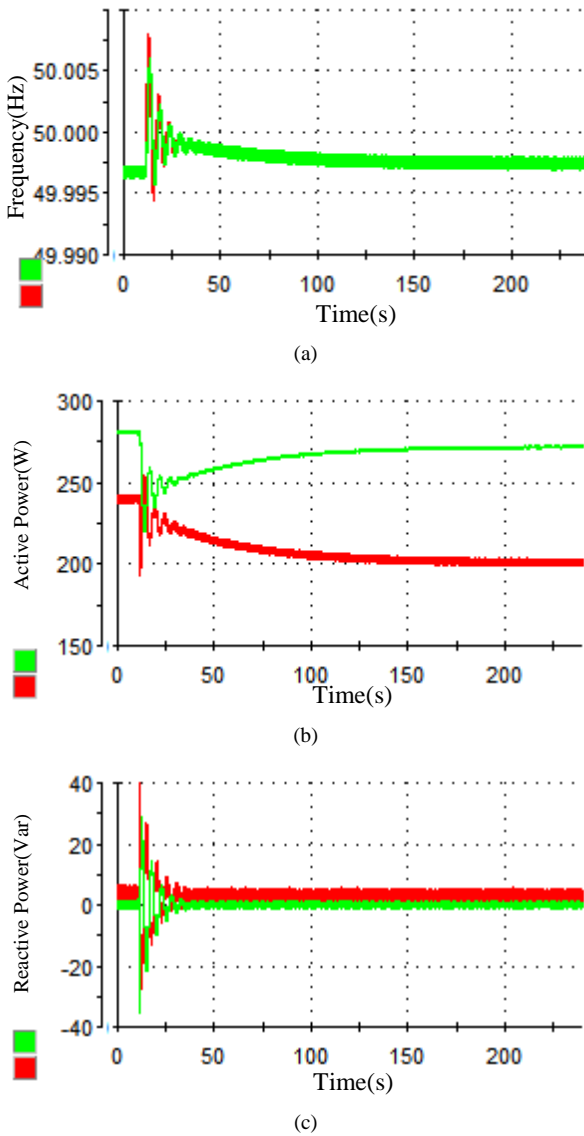

(a)

(b)

(c)

Fig. 15. Experimental results of active power transient responses during load disconnection disturbance: (a) frequency; (b) active power sharing; (c) reactive power sharing. Hydropower (red) and PV system (green)

VI. CONCLUSION

This paper proposed the use of hierarchical control to realize power sharing performance among VSIs and injecting the dispatched power to the hydroelectric power station simultaneously. In order to analyze the stability of the proposed hybrid microgrid system, state space models for both hydroelectric power and PV systems were developed. Root locus plots are also presented to help identifying the origin of each mode and to design the controller in a way to improve the system stability. Frequency stability simulation results were obtained from the demonstration hybrid microgrid under different scenarios and experimental results shown the effectiveness of the proposed approach.

REFERENCES

[1] Guerrero, J.M.; Poh Chiang Loh; Tzung-Lin Lee; Chandorkar, M., "Advanced Control Architectures for Intelligent Microgrids—Part II: Power Quality, Energy Storage, and AC/DC Microgrids," Industrial Electronics, IEEE Transactions on , vol.60, no.4, pp.1263,1270, April 2013

[2] Lasseter, R.H., "MicroGrids," Power Engineering Society Winter Meeting, 2002. IEEE , vol.1, no., pp.305-308, 2002

[3] Wu Chun Sheng; Liao Hua; Yang Zi Long; Wang Yi Bo; Peng Yan Chang; Xu Hong Hua."Research on control strategies of small-hydro/PV hybrid power system," Sustainable Power Generation and Supply, pp.1-5. 2009

[4] Beluco, A.; Souza, P.K.; Krenzinger,A.. "PV hydro hybrid systems," Latin America Transactions, IEEE, vol.6, no.7, pp. 626-631, 2008

[5] Guerrero, J.M.; Chandorkar, M.; Lee, T.; Loh, P.C., "Advanced Control Architectures for Intelligent Microgrids—Part I: Decentralized and Hierarchical Control," Industrial Electronics, IEEE Transactions on , vol.60, no.4, pp.1254,1262, April 2013

[6] Savaghebi, M.; Jalilian, A.; Vasquez, J.C.; Guerrero, J.M., "Secondary Control for Voltage Quality Enhancement in Microgrids," Smart Grid, IEEE Transactions on , vol.3, no.4, pp.1893,1902, Dec. 2012

[7] Chaoyong Hou, Xuehao Hu, Dong Hui, "Hierarchical Control Techniques Applied in Micro-grid," 2010 International Conference on Power System Technology, pp.1-5, Oct. 2010

[8] Prabha Kundur, Power Stability and Control, 1st ed., McGraw-Hill, 1994.

[9] P.K Olulope, K.A Folly, Ganesh K. Venayagamoorthy, "Modeling and simulation of hybrid distributed generation and its impact on transient stability of power system," Industrial Technology (ICIT), 2013 IEEE International Conference on, pp,1757-1762, Feb. 2013

[10] J. H. Zhou, P. L, X. H. Ge, X. S. Zhang, X. Q. Gao, Y. Liu, "Stability Simulation of a MW-Scale PV-Small Hydro Autonomous Hybrid System," Power and Energy Society General Meeting (PES), 2013 IEEE, pp.1-5, July 2013

[11] Wu Chun Sheng, Liao Hua, Yang Zi Long, Wang Yi Bo, Peng Yan Chang and Xu Hong Hua "Research on Control Strategies of Smaill-Hydro-PV Hybrid Power System," International Conference on Sustainable Power Generation and Supply, pp. 1-5, 2009

[12] NagarajuPogaku, Milan Prodanovic´, and Timothy C. Green, "Modeling, Analysis and Testing of Autonomous Operation of an Inverter-Based Microgrid". IEEE Trans Power Electronics, VOL. 22, NO. 2, MAR 2007

[13] F. Katiraei, M.R. Iravani and P.W. Lehn "Small-signal dynamic model of a micro-grid including conventional and electronically interfaced distributed resources". IET Gener. Transm. Distrib., 2007, 1, (3), pp. 369–378

[14] Thorne, D.H. , Hill, E.F. ,"Field Testing and Simulation of Hydraulic Turbine Governor Performance," Power Apparatus and Systems, IEEE Transactions on ,Vol.PAS-93, Issue,4, pp.1183-1191, July 1974